Open-closed field line boundary position: A parametric study using an MHD model

K. Kabin, R. Rankin, G. Rostoker, R. Marchand, and I. J. Rae
Department of Physics, University of Alberta, Edmonton, Alberta, Canada

A. J. Ridley, T. I. Gombosi, C. R. Clauer, and D. L. DeZeeuw
Space Physics Research Laboratory, University of Michigan, Ann Arbor, Michigan, USA

Received 29 July 2003; revised 26 March 2004; accepted 7 April 2004; published 28 May 2004.

[1] In this paper we investigate the effect of changes in the interplanetary magnetic field (IMF), solar wind dynamic pressure, and dipole tilt angle on the position of the ionospheric projection of the open-closed field line boundary (OCB) in a magnetohydrodynamic (MHD) model. We carry out a large number of steady state global MHD simulations in order to parameterize the OCB as a function of the solar wind B_y and B_z which we find to have the largest effect on the OCB location. We interpolate between the values produced by the simulations, which allows us to evaluate the location of the OCB projection into the ionosphere for any values of $|B_y| < 10$ nT and $|B_z| < 10$ nT. It is found that, particularly on the nightside, the OCB position is very sensitive to changes in the northward IMF component B_z, but it is much less sensitive to changes in B_z when it is southward. The response of the OCB location to changes in B_y also depends greatly on whether B_z is northward or southward, being much larger in situations in which $B_z > 0$ nT. We also find that the polar cap area increases with the increasing solar wind dynamic pressure. The B_x component of the IMF and the dipole tilt angle are found to have relatively small effects on the location of the OCB. *INDEX TERMS:* 2776 Magnetospheric Physics: Polar cap phenomena; 2736 Magnetospheric Physics: Magnetosphere/ionosphere interactions; 2740 Magnetospheric Physics: Magnetospheric configuration and dynamics; 2753 Magnetospheric Physics: Numerical modeling; *KEYWORDS:* open-closed field line boundary, polar cap dependence on interplanetary conditions, global MHD modeling

Citation: Kabin, K., R. Rankin, G. Rostoker, R. Marchand, I. J. Rae, A. J. Ridley, T. I. Gombosi, C. R. Clauer, and D. L. DeZeeuw (2004), Open-closed field line boundary position: A parametric study using an MHD model, *J. Geophys. Res.*, *109*, A05222, doi:10.1029/2003JA010168.

1. Introduction

[2] It is now well established that solar wind conditions determine to a large extent the size and shape of the Earth's magnetosphere. Since the pioneering work of *Dungey* [1961], a vast amount of observational evidence has been presented showing how the energy transfer process is regulated by the primary solar wind parameters of magnetic field and particle velocity and number density. The dependence of the magnetospheric configuration on the solar wind energy input has typically been discussed in terms of the convection flow patterns established in the magnetosphere and ionosphere, and in terms of the electric current systems that flow within the magnetosphere-ionosphere system [e.g., *Kamide*, 1988]. It is common to try to determine whether these flows and currents lie on the closed field lines of the magnetosphere, or on open field lines that connect directly to the magnetosheath. This requires the definition of the boundary that separates closed and open field lines, and a great deal of attention has been directed toward the identification of the particle and field signatures of this boundary. In this paper we address the issue of the open-closed field line boundary (OCB) location in an MHD model for various solar wind parameters.

[3] In addressing the question of the OCB location, we are equivalently exploring the size of the polar cap as defined by the area of the ionosphere threaded by open field lines. One of the early studies of this problem was by *Siscoe and Huang* [1985], who investigated the effect of unbalanced merging between the dayside and nightside regions. The existence of unbalanced merging led to either polar cap inflation or deflation depending on whether dayside merging was greater than nightside merging or vice versa, respectively. However, the authors simply took various merging rates as prescribed and did not consider the effects of individual solar wind and IMF parameters on the polar cap area. In an even earlier publication, *Voigt* [1974] investigated the OCB location by solving the Chapman-Ferraro problem for prescribed magnetopause shape and neutral sheet conditions. He found that the polar cap area grew in size as the magnetopause standoff distance de-

0148-0227/04/2003JA010168

creased and as the neural sheet approached the Earth. *Voigt* [1974] did not attempt to correlate the input parameters of his model to the solar wind and IMF conditions. *Birn et al.* [1991] looked at the OCB in the Tsyganenko 1987 magnetic field model in connection with unusual ''horse collar auroras.'' However, the definition of the OCB in the Tsyganenko 1987 model is somewhat arbitrary, so the authors considered a field line open if it extended beyond 70 R_E into the magnetotail, where R_E is the Earth's radius. *Birn et al.* [1991] found that under certain conditions, an arrowhead-shaped polar cap area exists, which might be associated with the horse collar auroras.

[4] In the years that followed, many researchers sought to find the location of the OCB using various observational signatures. *De la Beaujardière et al.* [1991] used Sondrestrmfjørd radar data and auroral arc motion in the radar field of view to establish the position and motion of the OCB in the nighttime hours together with the reconnection electric field strength. Their technique assumed that the OCB marked the poleward edge of precipitating particles. The auroral oval is also known to roughly coincide with this boundary and was used for estimating the OCB location as well [e.g., *Feldstein and Starkov*, 1970]. More recently, *Blanchard et al.* [1997] used the poleward edge of the auroral red line emissions on the nightside to define the OCB, working under the assumption that regions of red line emissions are on closed field lines. They demonstrated that the error of their approach is almost always smaller than 1.2° of magnetic latitude. Around the same time, *Lockwood* [1997] used the spectral properties of precipitating auroral ions to identify the position and motion of the dayside OCB. *Sotirelis et al.* [1998] used Defense Meteorological Satellite Program (DMSP) satellites to identify the OCB locations in their study of the open magnetic flux. In agreement with the expectations, they found that the open magnetic flux increased drastically for southward orientation of the IMF as compared with the northward case. All these studies looked only in specific local time regions and did not attempt to define the variation of the OCB over all local times and various solar wind conditions.

[5] It should be noted, however, that some studies in the past have used imager data to establish the polar cap boundary at all local times for intervals during which substorm expansive phase activity was taking place [e.g., *Frank and Craven*, 1988; *Brittnacher et al.*, 1999]. These studies, involving only the satellite-borne imager data, assumed that the boundary of the polar cap represented the locus where the auroral luminosity fell below some arbitrary threshold. These publications focused on the changes of auroral oval in response to specific substorm events. It also should be noted that the current space missions and ground-based instruments are capable of providing, in principle, the location of the polar cap boundary on a global scale. Recently, *Milan et al.* [2003] presented a global picture of the evolution of the OCB for a 7.5-hour interval on 5 June 1998. Such an exceptional experimental date coverage is still rather rare.

[6] The progress in the sophisticated MHD simulations of the solar wind/magnetosphere interaction also makes it possible to look at the character of the OCB in global terms. For example, a specific event was studied by *Elsen et al.* [1998], who compared the OCB obtained in a global MHD simulation with the poleward boundary of the auroral emissions measured by the ultraviolet imager on board the Polar spacecraft. *Raeder et al.* [1998] considered two events for which they find a generally good comparison of the open-closed field line boundary with the available experimental constraints. For another event, *Maynard et al.* [2003] studied magnetospheric response to a sudden interplanetary magnetic field (IMF) change. They also tracked the OCB for all local times during their simulation.

[7] Most recently, *Rae et al.* [2004] compared the OCB locations in the BATS-R-US MHD model (which is also the model used in the present study) to the poleward edges of the 630.0-nm emission for nine events when both the solar wind conditions and the auroral emissions were nearly constant for at least 2 hours. They found that the difference between the MHD modeled and observed OCB location was typically of the order of 1° latitude, which is about the same as the inherent error of using auroral emissions to locate this boundary. Events they have considered included both northward and southward IMF cases and corresponded to different values of B_y, B_x, and solar wind dynamic pressure. Because high-quality photometer measurements are usually obtained in the dusk-midnight sector, the model-data comparisons performed by *Rae et al.* [2004] mostly fall in the 1800–2400 MLT sector, with a few points in the postmidnight interval.

[8] To date, all the MHD results dealt only with the specific circumstances of individual events that were under investigation. In light of the fact that the identification of the OCB permits the area of the polar cap to be established, and that the polar cap area is a good proxy for the amount of magnetic flux stored in the tail lobes, it is valuable to establish the OCB position under different IMF and solar wind conditions. This paper is devoted to the study of that question for quiet magnetospheric conditions. Our motivation for this study is twofold. First, it follows from the comparison with the data by *Rae et al.* [2004] that our model usually provides an accurate estimation for the actual location of the open-closed field line boundary under steady magnetospheric conditions. Second, we feel that since MHD modeling has become a commonly available tool in the field of space science, it is important to document the complex behavior of such models even if their agreement with data is not always perfect. If the effects of various model input parameters on the OCB location are known, it should help a researcher in understanding and interpreting various other results (and, possibly, limitations) of his or her modeling.

2. Steady State Approximation to the Earth's Magnetosphere

[9] We use steady state MHD to describe the Earth's magnetosphere under stationary solar wind and IMF conditions. While solar wind and IMF parameters often change dynamically, periods of long nearly stationary conditions are also known to exist. For example, on 19–20 March 1999, there were some 14 hours of nearly steady southward IMF. It should be noted that stationary solar wind conditions do not guarantee that the magnetosphere is close to a steady state. In this case, often one or more substorms ensues, which leads to contractions and expansions of the polar cap.

Under these conditions, the OCB location exhibits hysteresis and depends not only on the current solar wind conditions, but also on the history of magnetospheric evolution. However, sometimes steady magnetospheric convection events occur which are known to have lasted for several hours. An extensive review of the observations pertaining to such events is given by *Sergeev et al.* [1996], who reference numerous publications regarding individual steady magnetospheric convection events. The physical conditions leading to steady magnetospheric convection events are not yet entirely understood; however, in a recent paper *O'Brien et al.* [2002] describe some of the statistics of their occurrence. The repeatability of auroras under similar quiet magnetospheric conditions was demonstrated by *Oznovich et al.* [1993], which lends further credibility to the concept of steady state in the context of our study. It is such cases of steady magnetospheric convection that are primary applications of this study.

[10] *Ridley et al.* [2002] used the BATS-R-US MHD code to model the global magnetosphere for three large storm events. These were the time periods in which the IMF had slow rotations from strongly southward IMF to strongly northward IMF. For each of these events, the ionospheric convection was directly compared to measurements by two DMSP satellites. Overall, there were over 150 passes of DMSP through the northern and southern polar caps. Root-mean-square (RMS) errors between measured and calculated convections velocities along the satellite trajectories were generated and examined. For one of the events, *Ridley et al.* [2002] compared the results of both a time-dependent simulation and a series of steady state snapshots to the measured data. They reported that there were only a few DMSP passes in which the RMS errors for the time-accurate run were significantly smaller than those for a quasi steady state approximation. This indicates that when the IMF is slowly rotating (even when it is rather large), the magnetospheric state can be approximated by a series of steady state models. *Ridley et al.* [2002] also noted that the location of the convection reversal boundary was well modeled throughout the intervals, even using the steady state approximation. This implies that the OCBs in the MHD model are approximately correct, since the convection reversal boundary has been shown to map to the low-latitude boundary layer [*Ridley and Clauer*, 1996, and references therein]. Finally, the favorable comparison with the data by *Rae et al.* [2004] shows directly that MHD simulations are capable of reproducing the OCB, at least under steady magnetospheric conditions.

[11] Obviously, when the IMF is changing rapidly or there are substorms, the steady state approximation is not appropriate. In this study we are modeling idealized, steady events. For these types of time periods, the *Ridley et al.* [2002] study shows that the magnetosphere can be approximated by a steady state solution, as we have done here. The response of the OCB to rapid changes in solar wind conditions will be addressed in a future publication.

3. MHD Model and Parameterization of the OCB

[12] In this study we use the BATS-R-US MHD model which is described by *Powell et al.* [1999] and *DeZeeuw et al.* [2000, and references therein]. This is the same MHD model which was successfully used in an earlier study of the OCB location [*Rae et al.*, 2004]. This model uses the single-fluid equations of ideal magnetohydrodynamics, which express the conservation of mass, momentum, and energy of plasma in a self-consistent magnetic field. While this description is generally believed to be adequate in the outer magnetosphere, it clearly breaks down in the inner magnetosphere where multifluid and kinetic effects become dominant. Work is currently under way to couple an ideal MHD model of the outer magnetosphere with an inner magnetosphere model similar to the Rice convection model [*DeZeeuw et al.*, 2003], but the results are not yet generally available. In particular, our model does not incorporate ring current or region II currents at present. Effects of the Earth rotation are also not included in our simulations. Ideal MHD also does not provide an adequate description of the Earth's ionosphere, where finite conductivity effects are important. The ionosphere in the model is represented by a two-dimensional layer with prescribed nonuniform Hall and Pederson conductivities. The distributions of the Hall and Pederson conductivities depend on the solar zenith angle and are explicitly given by *Ridley et al.* [2001, 2004]. A two-dimensional equation for the electric potential is solved in this conducting layer using a spherical grid with 65 points in the magnetic latitude and 256 points in the magnetic longitude. The magnetosphere-ionosphere coupling is achieved by importing field-aligned currents from the magnetospheric module into the ionospheric module and exporting the convection velocities in the opposite direction. This procedure is detailed in the same references. The inner boundary conditions in the model are imposed at 3 R_E. The magnetic field inside this radius is assumed to be a pure centered dipole with the equatorial strength of the magnetic field of $-31{,}100$ nT. The dipole magnetic field model is also used to map the ionospheric convection velocities and field-aligned currents between the ionosphere and the inner boundary of the magnetospheric simulation box. Our simulations were performed on an unstructured Cartesian grid with a typical size of 4×10^6 cells. The smallest cell size of our grid was 1/6 R_E. Such cells were located close to the Earth and near important magnetospheric interfaces, such as the magnetopause. The coordinate system used in the model is GSM: The X axis points from the Earth to the Sun, the Z axis is positive to the north and is in the plane which contains the X axis and the Earth's dipole, and the Y axis completes the right-hand system.

[13] As was discussed by *Powell et al.* [1999], our model does not use artificial dissipation; the stability of the scheme is achieved through solely numerical resistivity and viscosity. These are also the mechanisms responsible for the magnetic reconnection in the code.

[14] In our case studies, the MHD model is converged to a steady state for different choices of solar wind parameters. Then, the open-closed field line boundary is extracted from the steady state solutions. To identify the open-closed field line boundary, we trace a series of field lines originating on a particular magnetic meridian in the Northern Hemisphere. These field lines can belong to only two different types: They either go to the southern ionosphere (in which case they are closed) or go outside the bow shock (in which case they are open). The size of the simulation box ($256 \times 128 \times 128$ R_E) is large enough that no doubts in labeling the

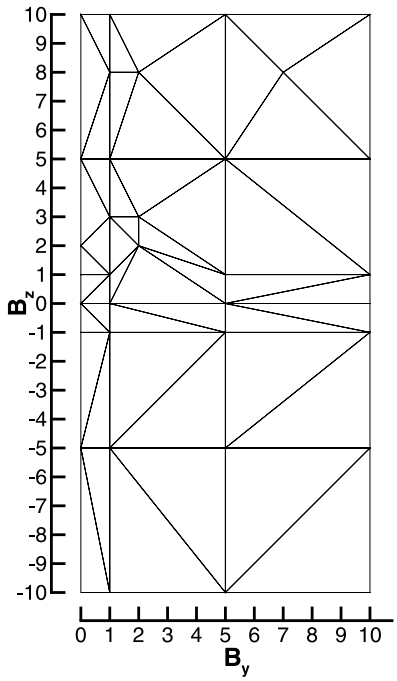

Figure 1. Grid in the B_y, B_z plane.

field line as either closed or open are possible. For the work presented in this paper we extracted the open-closed field line boundary with an accuracy of better than 0.2° in latitude in the ionosphere. We note that a latitude difference of 0.2° in the ionosphere corresponds to about 25 km, which is actually smaller than the smallest grid cell used in the model. Therefore we used linear interpolation for the magnetic field inside each cell, which is consistent with the second-order solution scheme [*Powell et al.*, 1999].

[15] Typically, we extract $N = 72$ points along the ionospheric projection of this boundary. However, it is not convenient to work directly with these discrete points because they are, in general, nonuniformly distributed along the open-closed field line boundary. We find that it is much more convenient to represent the projection of the open-closed field line boundary into the ionosphere with the coefficients of a Fourier expansion in a longitude-like variable. Therefore we apply the following procedure to the extracted boundary. Starting with the boundary given as a set of points $\{x_i,y_i|i = 1\ldots N\}$ in GSM coordinates, we first calculate the averages

$$x_{avg} = \frac{1}{N}\sum_{i=1}^{N} x_i \qquad y_{avg} = \frac{1}{N}\sum_{i=1}^{N} y_i$$

For any convex shape of the open-closed field line boundary, the point with coordinates x_{avg},y_{avg} lies inside the open field line domain. We use this point as a center of the new polar coordinate system r, ϕ'. We define ϕ' with respect to the positive direction of the GSM X axis. Then, we represent the open-closed field line boundary as

$$r(\phi') = a_0 + \sum_{i=1}^{k} (a_i \cos(\phi') + b_i \sin(\phi')). \qquad (1)$$

We find that using $k = 15$ in equation (1) gives a faithful reproduction of the open-closed field line boundary for all of the considered IMF conditions. With fewer coefficients, there might be noticeable deviations between the two boundaries, especially for northward IMF. For strong northward IMF the polar cap area may be quite extended in the noon-midnight direction and rather thin in the dawn-dusk direction. The coefficients a_i and b_i are computed using singular value decomposition to find a mean-square fit to an overdetermined system of equations

$$x_i = x_{avg} + r(\phi_i')\cos(\phi_i'), \quad y_i = y_{avg} + r(\phi_i')\sin(\phi_i'), \quad i = 1\ldots N.$$

[16] Once the coefficients of expansion (1) are computed for different IMF conditions, it is easy to interpolate these coefficients for any intermediate IMF values. Thus we obtain the open-closed field line boundary for the intermediate IMF conditions as well.

[17] Figure 1 shows the grid used in the B_y, B_z plane to interpolate the open-closed field line boundary for any intermediate values. We have performed a total of 35 MHD simulations for various combinations of B_y and B_z which form the nodes of the grid in Figure 1. These nodes were triangulated into a grid shown in Figure 1 using standard techniques [e.g., *Frey and George*, 1999]. We have put more nodes in the areas where the open-closed field line boundary is most sensitive to the IMF conditions. Then, the x_{avg}, y_{avg} values and the Fourier coefficients of equation (1) are linearly interpolated inside each triangle. The results of our model are mirror-symmetric with respect to the sign of B_y [*Tanaka*, 2001]; therefore we performed the calculations only for $B_y \geq 0$ and extended the results to the $B_y < 0$ half-plane.

[18] At present, we have developed only a model which is capable of interpolating the OCB for arbitrary values of B_y and B_z. In this paper we show that these are the most important parameters, although the OCB depends also on the dynamic pressure in the solar wind, dipole tilt angle, and the B_x component of the IMF. In the future, our model may be extended to include the dependence on these parameters as well, but at present it is not yet feasible to extend our analysis to adequately cover this five-dimensional parameter space.

4. Dependence of the Open-Closed Field Line Boundary on IMF B_y and B_z

[19] In what follows, we perform a detailed analysis of the OCB dependence on the B_y and B_z IMF components for "nominal" solar wind plasma parameters: $n = 5$ cm^{-3}, $U = 500$ km/s, and $T = 15$ eV.

[20] Figure 2 shows the variation of the open-closed field line boundary with the B_y component of the IMF for weakly northward IMF $B_z = 1$ nT. The OCBs shown in Figure 2 correspond to B_y changing from 0 to 10 nT in increments of 2 nT. Figure 3 is similar but for weakly southward IMF $B_z = -1$ nT. One can clearly see that for northward IMF the polar cap area increases greatly with increasing B_y for small values of that parameter. For large values of B_y, the changes in the location of the polar cap boundary are comparatively small. In general, increasing B_y causes the polar cap area to

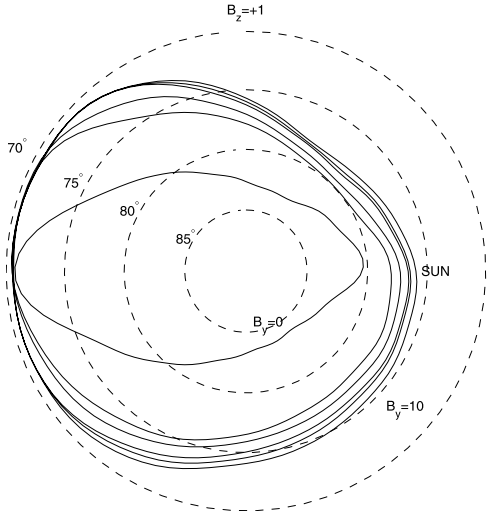

Figure 2. Open-closed field line boundary for B_z = 1 nT (northward) and B_y = 0, 2, 4, 6, 8, 10 nT. Dashed circles show magnetic latitudes separated by 5°.

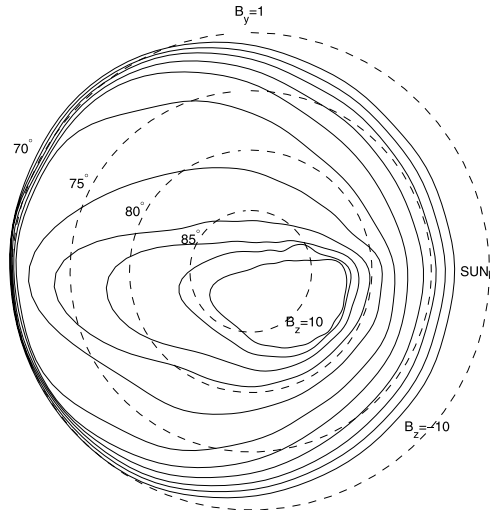

Figure 4. Open-closed field line boundary for B_y = 1 nT and B_z = −10, −8, −6, −4, −2, 0, 2, 4, 6, 8, 10 nT. Dashed circles show magnetic latitudes separated by 5°.

expand mostly through broadening in the dawn-dusk direction. At the same time, the OCB hardly changes at all on the nightside.

[21] The changes in the polar cap area associated with B_y are much smaller for weakly southward IMF, as illustrated by Figure 3. As B_y increases, the polar cap area bulges to lower geomagnetic latitudes on the dawnside, while the duskside and nightside are essentially the same for all B_y.

[22] Figure 4 shows the changes in the OCB for fixed B_y = 1 nT and B_z changing from +10 nT (strong northward) to −10 nT (strong southward) in increments of 2 nT. One can see how the polar cap areas vary from extremely small to fairly large as B_z changes. It is interesting to point out that as the B_z component of the magnetic field changes from strongly northward to weakly northward, the boundary drastically moves to lower latitudes on the nightside. However, as the IMF B_z component changes from weakly northward to strongly southward, the growth of the polar cap area on the nightside is virtually absent, but still continues on the dayside.

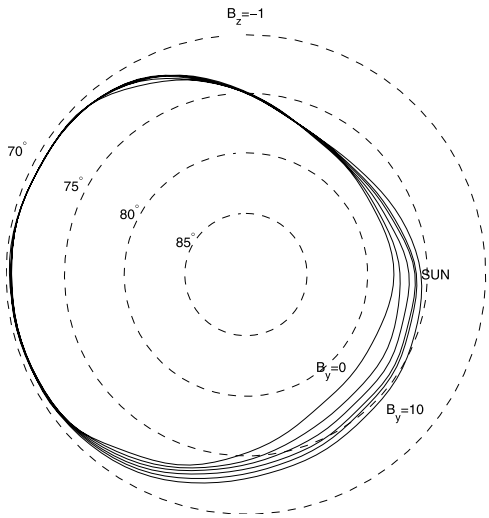

Figure 3. Open-closed field line boundary for B_z = −1 nT (southward) and B_y = 0, 2, 4, 6, 8, 10 nT. Dashed circles show magnetic latitudes separated by 5°.

[23] This may be explained as follows: A significant problem in most global MHD codes is the lack of stretching in the near-Earth magnetotail. The primary cause of this is the imbalance between the gradient in pressure force and the $J \times B$ force; in the near-Earth tail, the gradient in pressure is not large enough to hold the oppositely directed magnetic field lines above and below the plasma sheet apart. This is caused by either too large a pressure in the lobes or too small a pressure in the plasma sheet, which decreases the gradient in pressure between the lobes and the plasma sheet. Of these two possibilities, we feel that the second one is more likely, since the transport of the solar wind plasma across the bow shock and magnetosheath is probably well described using an MHD formalism. The lack of an adequate inner magnetosphere model may be critical for a realistic description of the plasma sheet.

[24] The thermal pressure distribution and magnetic field lines in the noon-midnight meridional plane for northward and southward IMF are illustrated in Figure 5. The right panel of this figure corresponds to B_z = 5 nT and B_y = 1 nT, while the left one corresponds to B_z = −5 nT and B_y = 1 nT. One can see that the pressure distribution in the plasma sheet on the nightside for the two cases is generally quite similar, in contrast to the dayside and cusp areas, where the pressure differs significantly for these two cases. For northward IMF the pressure in the plasma sheet only affects stretching of the magnetic field in the X = −10–20 R_E area but has little effect on the reconnection process which occurs in the high-latitude areas, near X = 0, Y = ±15 R_E. In contrast, for southward IMF, the plasma flow is pushed toward the plasma sheet in the tail and the reconnection takes place as soon as the plasma sheet pressure cannot withstand the dynamic pressure of the plasma in the lobes. Although many not entirely understood properties, such as anomalous resistivity [e.g., *Roussev et al.*, 2002], have some effect on the reconnection process, in our model the

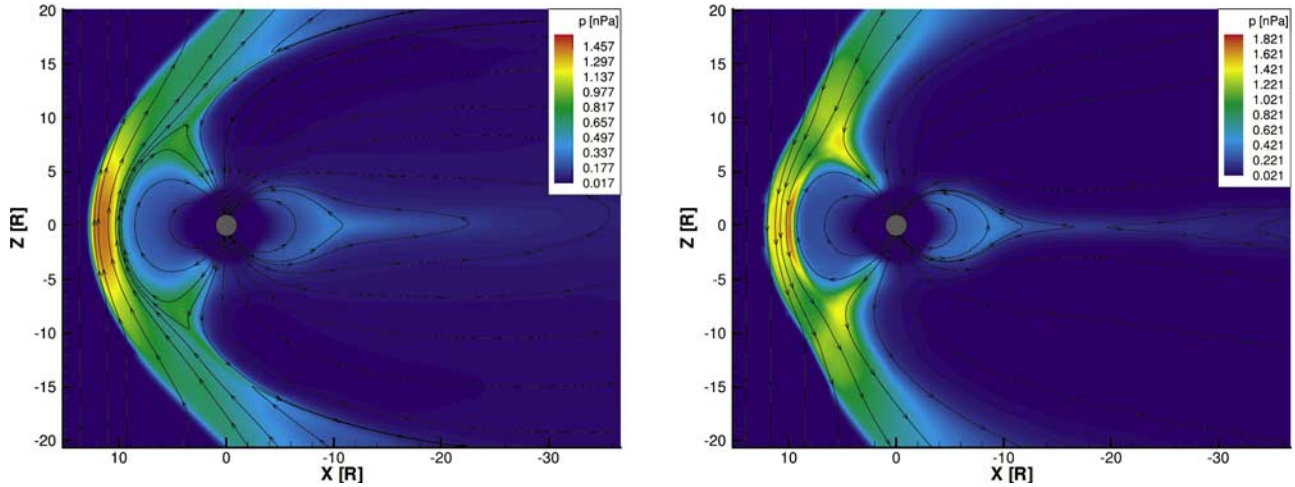

Figure 5. Pressure (color code) and the magnetic field lines in the north-south plane for (left) $B_z = 5$ nT, $B_y = 1$ nT and (right) $B_z = -5$ nT, $B_y = 1$ nT.

pressure balance plays the primary role. In our MHD simulation the tail reconnection for southward IMF happens at around $X = -15$ to -20 R_E which is closer to the Earth than most observations suggest. We believe that this happens because in our code we do not have an adequate model of the inner magnetosphere and plasmasphere. As a result, we do not have adequate pressure in the plasmasphere and tail region, which, in turn, leads to an insufficient stretching of the tail. Thus our simulations appear to represent quiet time periods when there is little energy stored in the tail. As a consequence of this feature of MHD models, it is relatively difficult to get a realistic energy storage and release cycle within an MHD code. More relevant for this study is the fact that the position of the OCB on the nightside is relatively independent of B_z, once B_z becomes negative. As explained above, we conclude that the nightside OCB within the MHD code most likely represents quiet periods, such as the start of the recovery phase of a large substorm. At that time, the amount of stored magnetic energy in the magnetotail is relatively small, representing a minimum energy solution, similar to the steady state MHD solutions. At the same time, we would like to point out that several of the events considered by *Rae et al.* [2004] involved southward IMF and OCB locations near midnight and the data-model comparison for these cases was still good.

5. The Effect of the Solar Wind Dynamic Pressure

[25] Figure 6 shows the open-closed field line boundary for two different solar wind conditions with the same dynamic pressure. The IMF was the same for these two runs: $B_y = 7$ nT and $B_z = 8$ nT. The boundary shown with circles corresponds to $n = 5$ cm^{-3} and $U = 500$ km/s while the solid line corresponds to $n = 10$ cm^{-3} and $U = 353.55$ km/s. Although solar wind velocities and densities are different, the dynamic pressure is the same in both cases. Figure 6 suggests that the OCB depends on the dynamic pressure of the solar wind, rather than on the solar wind density and velocity separately. The indentation on the dawnside in one of the boundaries is numerical in origin and is associated with a resolution change in the model run.

[26] Figure 7 shows the effect of changing solar wind dynamic pressure on the polar cap. For these three simulations, the conditions were $B_y = 5$, $B_z = -5$, $n = 5$ cm^{-3}, and $U = 300$, 500, and 800 km/s. Figure 8 is similar to Figure 7, but for northward IMF conditions: $B_y = 7$, $B_z = 8$. The solar wind dynamic pressure in either case increased from smallest to largest solar wind speed by a factor of more than 7. For northward IMF, in contrast to the southward case, the polar cap expansion is not uniform for all longitudes. In fact, there is not much change on the dawnside at all, while the day, night, and dusk sides expand equatorward. The polar cap areas increase with the increasing solar wind dynamic pressure because at higher dynamic pressure levels the merging field lines either at the dayside magnetopause (for southward IMF) or in the cusp areas (for northward IMF) are pushed harder toward each other and

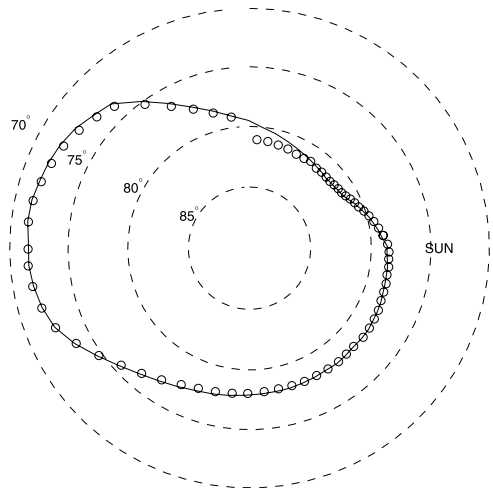

Figure 6. Open-closed field line boundary for two different solar wind conditions with the same dynamic pressure. Solid line corresponds to $n = 10$ cm^{-3}, $U = 353.55$ km/s, and circles correspond to $n = 5$ cm^{-3}, $U = 500$ km/s.

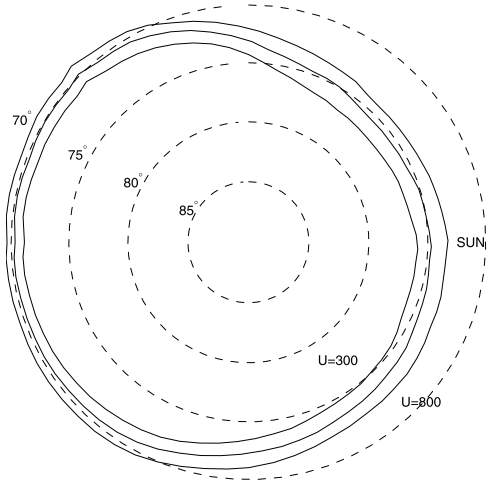

Figure 7. Open-closed field line boundary for B_y = 5 nT, B_z = −5, nT n = 5 cm^{-3}, and U = 300, 500, and 800 km/s.

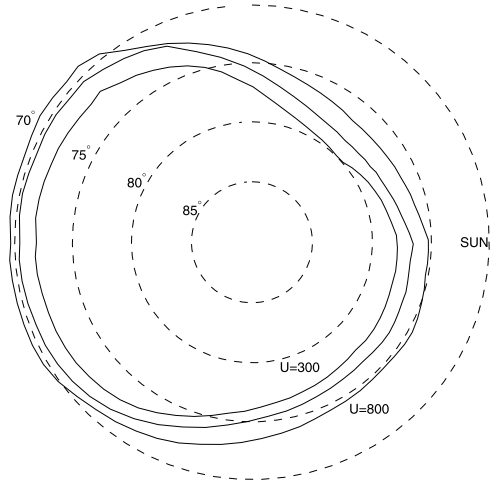

Figure 9. Open-closed field line boundary for B_y = 5 nT, B_z = 0 nT, n = 5 cm^{-3}, and U = 300, 500, and 800 km/s.

as a result the reconnection rate in the model can only grow larger. For the model runs from which Figures 7 and 8 were produced, the polar cap size was influenced by reconnection involving both the B_y and B_z components of the IMF. For purely northward IMF, however, the polar cap area is extremely small and may be virtually independent of solar wind dynamic pressure.

[27] Figure 9 illustrates the effect of the solar wind dynamic pressure on the OCB for the case when the IMF has only a B_y component. The polar cap expansion for different MLTs in this case is mostly uniform and, in that sense, is similar to the southward IMF case. The U = 500 and 800 km/s contours in Figure 9 do, however, pass very close to each other on the dawnside, which indicates that the pure B_y case has features somewhat intermediate between northward and southward IMF cases.

[28] The dynamic pressure of the solar wind can obviously change the polar cap area, although its effect is not nearly as strong as that produced by changes in the B_y and B_z components of the solar wind in some regimes. The polar cap area for the three cases with different solar wind speeds shown in Figure 7 for southward IMF are 0.26, 0.29, and 0.33 R_E^2 (see section 9 for the description of the area calculation), respectively. For pure IMF B_y (Figure 9) the corresponding areas are 0.20, 0.24, and 0.28 R_E^2, and for northward IMF (Figure 8) they are 0.14, 0.16, and 0.20 R_E^2. Thus one can say that increasing the solar wind dynamic pressure by a factor of 7 expands the polar cap area by 30–40%, and this expansion is larger for northward than for southward IMF.

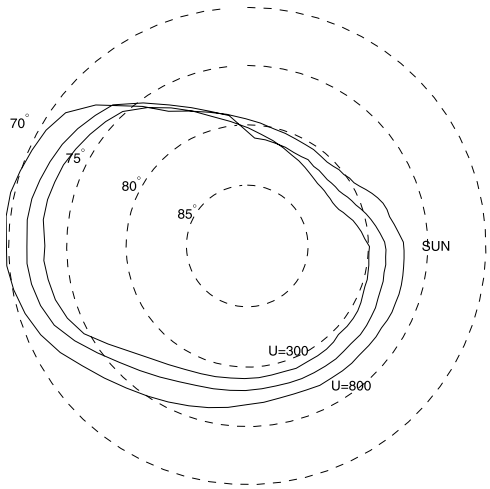

Figure 8. Open-closed field line boundary for B_y = 7 nT, B_z = 8 nT, n = 5 cm^{-3}, and U = 300, 500, and 800 km/s.

6. The Effect of the Dipole Tilt

[29] The tilt of the Earth's magnetic dipole in the GSM coordinate system changes from about −33° (winter, night) to about +33° (summer, day). This variation adds an additional dimension to the parameter space of the problem

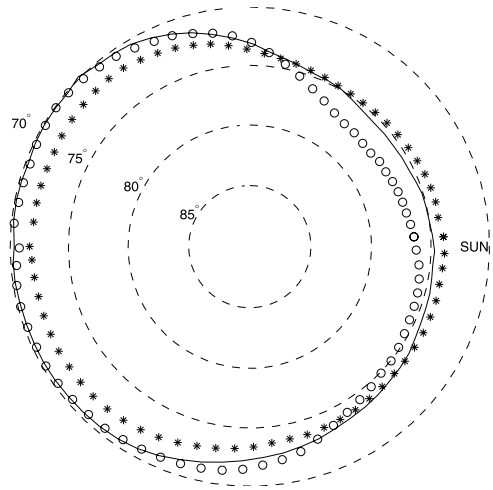

Figure 10. Open-closed field line boundary for dipole tilt angles θ = 0° (solid line), θ = −35° (circles), and θ = 35° (stars) in geomagnetic coordinates. Solar wind parameters are n = 5 cm^{-3}, U = 500 km/s, T = 15 eV, B_y = 5 nT, and B_z = −5 nT.

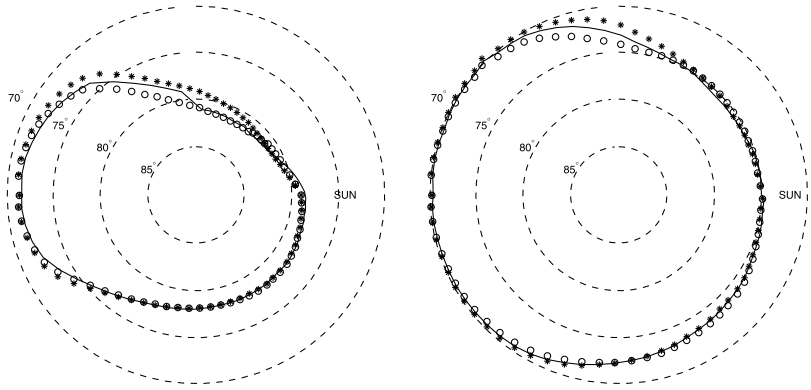

Figure 11. Effect of the B_x component of the IMF. (left) Northward IMF, B_y = 7, B_z = 8 nT. (right) Southward IMF, B_y = 5, B_z = −5 nT. In both panels the solid line corresponds to B_x = 0 nT, stars correspond to B_x = +10 nT, and open circles correspond to B_x = −10 nT.

studied in this paper. It is known, however, that the OCB is centered, to a first order, relative to the geomagnetic pole [*Feldstein and Starkov*, 1970; *Oznovich et al.*, 1993]. In particular, *Oznovich et al.* [1993] experimentally found that if the dipole tilt angle changes by 10°, then the latitude of the auroral emissions changes only by about 1°. Below, we quantify similar findings in an MHD model. Under this assumption, the OCB location in GSM coordinates can be simply rotated by the change in the dipole tilt angle.

[30] Figure 10 shows the results of MHD calculations with dipole tilts of θ = ±35° and θ = 0° in geomagnetic coordinates. The center of the plot corresponds to the magnetic pole for all three simulations; positive θ corresponds to the summer hemisphere. The solar wind conditions for all these simulations were n = 5 cm^{-3}, U = 500 km/s, T = 15 eV, B_y = 5 nT, and B_z = −5 nT. We note that the largest differences in the OCB positions between tilted and nontilted dipole cases are on the nightside if the magnetic dipole axis is tilted away from the Sun, and on the dayside if the axis is tilted toward the Sun. However, even for the extreme values of the dipole tilt, the differences between the open-closed field line boundaries are quite small, of the order of 1°–2° of magnetic latitude. This change in the location of the OCB is of the same order of magnitude as that obtained by *Oznovich et al.* [1993] in their study of seasonal effects on auroral emissions.

7. Effect of the B_x Component of the IMF

[31] The B_x component of the IMF also has some effect on the location of the OCB; however, this effect is usually considerably smaller than that of the B_y and B_z components. The only case when the B_x component may have a dominant effect on the OCB location is strong northward IMF with a small B_y component when very unusual OCB shapes may occur [*Crooker*, 1992]. We do not investigate this particular combination of the upstream parameters in this paper.

[32] Figure 11 shows the results for using B_x = ±10 nT in the upstream boundary conditions. The left plot of Figure 11 corresponds to northward IMF with B_y = 7, B_z = 8 nT, n = 5 cm^{-3}, and U = 500 km/s. The right plot is for southward IMF with B_y = 5, B_z = −5 nT, n = 5 cm^{-3}, and U = 500 km/s. One can see that changing B_x by up to 10 nT has very little effect on the OCB in either case. In both cases the changes are the largest in the dusk sector, while for other local times the OCB hardly changes at all.

8. Polar Cap in the Southern Hemisphere

[33] Until now, we have investigated only the ionospheric projection of the OCB into the Northern Hemisphere. The polar cap, of course, exists in the Southern Hemisphere as well. Figure 12 shows the open-closed field line boundaries in the two hemispheres for B_y = 1, B_z = 5 nT, n = 5 cm^{-3}, and U = 500 km/s. The OCB for the Northern Hemisphere is shown in Figure 12 by the solid line and in the Southern Hemisphere by the dash-dotted line. The two polar caps are simply the mirror images of each other with respect to the noon-midnight meridian plane. This comes as no surprise because for positive B_y the merging occurs on the duskside in the Northern Hemisphere and on the dawnside in the Southern Hemisphere (the merging locations are reversed for negative B_y). In the absence of the B_y component the

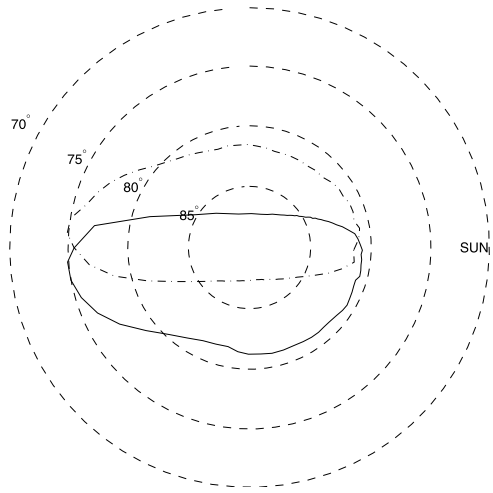

Figure 12. Open-closed field line boundaries for Northern (solid line) and Southern (dash-dotted line) Hemispheres for B_y = 1 and B_z = 5 nT.

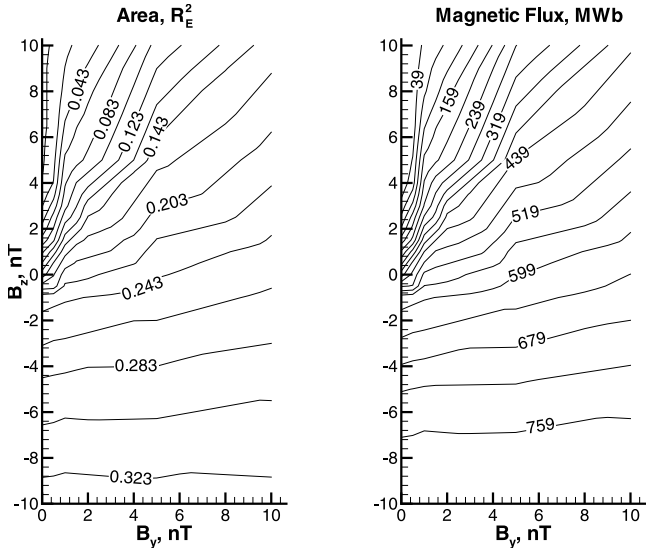

Figure 13. (left) Polar cap area and (right) open magnetic flux, as functions of B_y and B_z.

MHD solution is symmetric with respect to the noon-midnight meridional plane.

[34] Using the expected mirror symmetry between the Northern and Southern Hemispheres (which is confirmed by Figure 12), we can use the model described in sections 3 and 4 to compute the ionospheric projection of the OCB in the Southern Hemisphere as well.

9. Calculation of the Polar Cap Area

[35] The area of a surface element of a unit sphere is given by

$$dS = d\phi \cos(\theta) d\theta$$

where ϕ is the longitude and θ is the latitude. Thus, if the location of the ionospheric projection of the OCB is known, the polar cap area can be easily calculated numerically.

[36] In addition to the polar cap area, it is often useful to know the magnetic flux through the polar cap. This flux can be calculated as

$$\Phi = \int \int_S B_r dS$$

where B_r is the radial component of the Earth's intrinsic magnetic field. In particular, the magnetic flux through the whole Northern Hemisphere is $\Phi_{\text{total}} = 2\pi B_0 R_E^2 \approx 8 \times 10^3$ MWb assuming that the Earth's internal magnetic field is purely dipole. Here B_0 is the strength of the dipole field at the magnetic equator.

[37] The left panel of Figure 13 shows the polar cap area as a function of B_y and B_z. The polar cap area is the smallest for large northward IMF with a small B_y component. In fact, for purely northward IMF our MHD model predicts a closed magnetosphere for $B_z > 3$ nT. For northward IMF the area of the polar cap depends strongly on the B_y magnitude. In contrast, for strong southward IMF, the area is almost independent of B_y. The right panel of Figure 13 shows the magnetic flux through the polar cap.

10. Conclusions

[38] In this paper we have presented results of a systematic study of the OCB in a global MHD model of the Earth's magnetosphere. A recent comparison with observations reported by *Rae et al.* [2004], who used the same MHD model as the present work, implies that our model provides a good description of the OCB when the Earth's magnetosphere is in steady state. Here we have investigated the effects of B_x, B_y, and B_z components of the IMF, the solar wind dynamic pressure, and the tilt of the Earth dipole axis.

[39] We find that as the B_z component of the IMF changes from northward to southward the polar cap area increases, as expected. However, once the IMF is southward we find little expansion of the polar cap on the nightside, which we attribute to the nature of the steady state MHD model. As discussed in section 4, steady state MHD equations describe a magnetospheric configuration with minimum energy, which physically corresponds to the quiet state of the magnetosphere, for example, after a major substorm.

[40] Increasing the solar wind dynamic pressure in our model leads to a growth in the area of the open field lines threading the polar ionosphere. For southward IMF, this expansion of the polar cap area is essentially uniform for all MLTs, while for northward IMF with nonzero B_y this expansion is somewhat nonuniform. The effects of changing IMF B_x on the location of the OCB in general are found to be small. We find that changing the dipole tilt angle in the GSM coordinates by 35°, which is the largest possible amount, results only in a 1°–2° latitude change in the OCB location in the geomagnetic coordinates.

[41] We feel that a model of the type described in this paper is needed by the space physics community. Although global MHD calculations are becoming more and more accessible with the increase of the readily available computer power, they are still quite demanding in terms of resources, both computer and human. A model which simply interpolates the open closed field line boundary using a large library of precomputed MHD solutions requires negligible computing power and can be easily used by any researcher. It is our intention to make such a model publicly available though the World Wide Web.

[42] **Acknowledgments.** The University of Alberta group was supported in part by the Canadian Space Agency and by the Natural Sciences and Engineering Research Council of Canada. The Michigan group was supported by the ITR NSF grant ATM-0325332, NASA grant NAG 510504, and by DOD MURI grant F49620-01-1-0359. We also acknowledge the use of WestGrid computational resources.

[43] Arthur Richmond thanks Steve E. Milan and another reviewer for their assistance in evaluating this paper.

References

Birn, J., E. W. Hones Jr., J. D. Craven, L. A. Frank, R. D. Elphinstone, and D. P. Stern (1991), On open and closed field line regions in Tsyganenko's field model and their possible associations with horse collar auroras, *J. Geophys. Res.*, *96*, 3811–3817.

Blanchard, G. T., L. R. Lyons, and J. C. Samson (1997), Accuracy of using 6300 Å auroral emission to identify the magnetic separatrix on the nightside of Earth, *J. Geophys. Res.*, *102*, 9697–9703.

Brittnacher, M., M. Fillingim, G. Parks, G. Germany, and J. Spann (1999), Polar cap area and boundary motion during substorms, *J. Geophys. Res.*, *104*, 12,251–12,262.

Crooker, N. U. (1992), Reverse convection, *J. Geophys. Res.*, *97*, 19,363–19,372.

de la Beaujardière, O., L. R. Lyons, and E. Friis-Christensen (1991), Sondrestrøm radar measurements of the reconnection electric field, *J. Geophys. Res.*, *96*, 13,907–13,912.

DeZeeuw, D. L., T. I. Gombosi, C. P. T. Groth, K. G. Powell, and Q. F. Stout (2000), An adaptive MHD method for global space weather simulations, *IEEE Trans. Plasma Sci.*, *28*, 1956–1965.

DeZeeuw, D., S. Sazykin, R. Wolf, M. Liemohn, T. Gombosi, and K. Powell (2003), Inner magnetosphere results from coupled MHD-RDM modeling, *Eos Trans. AGU*, *84*(46), Fall Meet. Suppl., Abstract SM22A-0226.

Dungey, J. W. (1961), Interplanetary magnetic field and the auroral zones, *Phys. Rev. Lett.*, *6*, 47–48.

Elsen, R. K., R. M. Winglee, J. F. Spann, G. A. Germany, M. Brittnacher, and G. K. Parks (1998), The auroral oval boundaries on January 10, 1997: A comparison of global magnetospheric simulations with UVI images, *Geophys. Res. Lett.*, *25*, 2585–2588.

Feldstein, Y. I., and G. V. Starkov (1970), The auroral oval and the boundary of closed field lines of geomagnetic field, *Planet. Space Sci.*, *18*, 501–508.

Frank, L. A., and J. D. Craven (1988), Imaging results from Dynamics Explorer 1, *Rev. Geophys.*, *26*, 249–283.

Frey, P. J., and P.-L. George (1999), *Maillages*, Hermes Sci., Paris.

Kamide, Y. (1988), *Electrodynamic Processes in the Earth's Ionosphere and Magnetosphere*, Kyoto Sangyo Univ. Press, Kyoto, Japan.

Lockwood, M. (1997), Relationship of dayside auroral precipitations to the open-closed separatrix and the pattern of convective flow, *J. Geophys. Res.*, *102*, 17,475–17,487.

Maynard, N. C., et al. (2003), Responses of the open-closed field line boundary in the evening sector to IMF changes: A source mechanism for Sun-aligned arcs, *J. Geophys. Res.*, *108*(A1), 1006, doi:10.1029/2001JA000174.

Milan, S. E., M. Lester, S. W. H. Cowley, K. Oksavik, M. Brittnacher, R. A. Greenwald, G. Sofko, and J.-P. Villain (2003), Variations in polar cap area during two substorm cycles, *Ann. Geophys.*, *21*, 1121–1140.

O'Brien, T. P., S. M. Thompson, and R. L. McPherron (2002), Steady magnetospheric convection: Statistical signatures in the solar wind and *AE*, *Geophys. Res. Lett.*, *29*(7), 1130, doi:10.1029/2001GL014641.

Oznovich, I., R. W. Eastes, R. E. Huffman, M. Tur, and I. Glaser (1993), The aurora at quiet magnetospheric conditions: Repeatability and dipole tilt angle dependence, *J. Geophys. Res.*, *98*, 3789–3797.

Powell, K. G., P. L. Roe, T. J. Linde, T. I. Gombosi, and D. L. DeZeeuw (1999), A solution-adaptive upwind scheme for ideal magnetohydrodynamics, *J. Comput. Phys.*, *154*, 284–309.

Rae, I. J., K. Kabin, R. Rankin, F. R. Fenrich, W. Liu, J. A. Wanliss, A. J. Ridley, T. I. Gombosi, and D. L. DeZeeuw (2004), Comparison of photometer and global MHD determination of the open-closed field line boundary, *J. Geophys. Res.*, *109*, A01204, doi:10.1029/2003JA009968.

Raeder, J., J. Berchem, and M. Ashour-Abdalla (1998), The geospace environment modeling grand challenge: Results from a global geospace circulation model, *J. Geophys. Res.*, *103*, 14,787–14,797.

Ridley, A. J., and C. R. Clauer (1996), Characterization of the dynamic variations of the dayside high-latitude ionospheric convection reversal boundary and relationship to interplanetary magnetic field orientation, *J. Geophys. Res.*, *101*, 10,919–10,938.

Ridley, A. J., D. L. DeZeeuw, T. I. Gombosi, and K. G. Powell (2001), Using steady state MHD results to predict the global state of the magnetosphere-ionosphere system, *J. Geophys. Res.*, *106*, 30,067–30,076.

Ridley, A. J., K. C. Hansen, G. Tóth, D. L. DeZeeuw, T. I. Gombosi, and K. G. Powell (2002), University of Michigan MHD results of the Geospace Global Circulation Model metrics challenge, *J. Geophys. Res.*, *107*(A10), 1290, doi:10.1029/2001JA000253.

Ridley, A. J., T. I. Gombosi, and D. L. DeZeeuw (2004), Ionospheric control of the magnetosphere: Conductance, *Ann. Geophys.*, *22*, 567–584.

Roussev, I., K. Galsgaard, and P. G. Judge (2002), Physical consequences of the inclusion of anomalous resistivity in the dynamics of 2D magnetic reconnection, *Astron. Astrophys.*, *382*, 639–649.

Sergeev, V. A., R. J. Pellinen, and T. I. Pulkkinen (1996), Steady magnetospheric convection: A review of recent results, *Space Sci. Rev.*, *75*, 551–604.

Siscoe, G. L., and T. S. Huang (1985), Polar cap inflation and deflation, *J. Geophys. Res.*, *90*, 543–547.

Sotirelis, T., P. T. Newell, and C. I. Meng (1998), Shape of the open-closed boundary of the polar cap as determined from observations of precipitating particles by up to four DMSP satellites, *J. Geophys. Res.*, *103*, 399–406.

Tanaka, T. (2001), Interplanetary magnetic field B_y and auroral conductance effects on high-latitude ionospheric convection patterns, *J. Geophys. Res.*, *106*, 24,505–24,516.

Voigt, G.-H. (1974), Calculation of the shape and position of the last closed field line boundary and the coordinates of the magnetopause neutral points in a theoretical magnetospheric field model, *J. Geophys.*, *40*, 213–228.

C. R. Clauer, D. L. DeZeeuw, T. I. Gombosi, and A. J. Ridley, Space Physics Research Laboratory, University of Michigan, Ann Arbor, MI 48109-2143, USA.

K. Kabin, R. Marchand, I. J. Rae, R. Rankin, and G. Rostoker, Department of Physics, University of Alberta, Edmonton, Alberta, Canada T6G 2J1. (kabin@phys.ualberta.ca)